Understanding the Phase Transitions of the Ni_2MnGa Magnetic Shape Memory System from First Principles

M. A. Uijttewaal,[1,*] T. Hickel,[1] J. Neugebauer,[1] M. E. Gruner,[2] and P. Entel[2]

[1]*Max-Planck-Institut für Eisenforschung GmbH, D-40237, Düsseldorf, Germany*

[2]*Physics Department and CENIDE, University of Duisburg-Essen, Campus 47048 Duisburg, Germany*

(Received 22 September 2008; revised manuscript received 10 November 2008; published 22 January 2009)

The free energies of the austenite, the (modulated) premartensite and the unmodulated martensite of Ni_2MnGa are determined using density functional theory and including quasiharmonic phonons *and* fixed-spin-moment magnons. This approach very well reproduces the complete phase sequence (martensite ↔ premartensite ↔ austenite) of stoichiometric Ni_2MnGa as a function of temperature. By analyzing the relevant free energy contributions, we also understand the delicate interplay of phonons and magnons driving both phase transitions.

DOI: 10.1103/PhysRevLett.102.035702 PACS numbers: 64.60.Ej, 63.20.dk, 75.50.Cc, 81.30.Kf

The Heusler alloy Ni_2MnGa belongs to a class of materials showing the magnetic shape memory (MSM) effect. In contrast to conventional shape memory alloys, where the change in shape is controlled solely by temperature, MSM alloys allow a control also by magnetic fields thus enabling switching frequencies in the kHz regime. The MSM effect is directly related to a martensitic phase transition. The high temperature (austenitic) phase is cubic, whereas in the low temperature (martensitic) phase the crystal symmetry is reduced by a tetragonal distortion and, consequently, the shape of the material changes. Near-stoichiometric Ni_2MnGa additionally shows a (modulated, but still cubic) premartensitic phase in between the austenite and the martensite. It has a tweed structure of $3M$ nature and is stable between the martensitic ($T_M \approx 200$ K) and the premartensitic transition temperature ($T_{PM} = 247$ K [1], respectively, 260 K [2]). For practical applications, T_M has to be well above room temperature, which can be achieved by changing the stoichiometry [3].

A thorough understanding of the physical mechanisms driving the phase transitions is required to perform a more systematic search for improved alloys. Recently, ultraviolet photoelectron spectroscopy (UPS) measurements of the changes in the electronic structure were reported going from the austenite to the martensite [1]. These confirm the formation of a pseudogap a little below the Fermi level as earlier determined from first principles [4,5]. The pseudogap forms the electronic basis of the stabilization of the martensite and the premartensite at lower temperatures. The pseudogap is formed by a reconstruction of minority spin Ni-d states around the Fermi level and this is understood from a combination of Fermi surface nesting [5] and a band Jahn-Teller effect [6–8]. Lee *et al.* [9] investigated the Fermi surface nesting in the austenite as a function of magnetization using the Stoner approximation. They found a pronounced peak in the generalized susceptibility of the majority spin channel at a wave vector of $\mathbf{q} = X_2/3$ for the experimental magnetic moment at the premartensite transition temperature, confirming the $3M$ nature of the premartensite.

To understand the phase transitions, however, the *thermodynamic* stabilization of the austenite and premartensite needs to be quantitatively determined. In this Letter, we, therefore, explicitly compute the relevant entropic contributions separately from first principles. This allows us to quantify and explain the mechanisms driving the phase transitions. A first attempt in this direction was undertaken by Enkovaara *et al.* [10] who treated the vibrational effects within the Debye approximation and obtained a realistic prediction for the transition temperature between the martensite and austenite phase ($T_M \approx 175$ K). To keep the numerical effort tractable, the study, however, did not take into account the intermediate modulated premartensite phases as well as the influences of the temperature dependent magnetization on structural stability [11].

Within this Letter, we overcome both shortcomings and find a very good agreement of the respective transition temperatures. An analysis of the different contributions demonstrates that finite temperature magnetic effects are necessary to explain the premartensite transition, whereas the martensite transition is driven by combined vibrational and magnetic excitations.

The present study employs density functional theory (DFT) within the generalized gradient approximation [12]. We use the Vienna *ab initio* simulation package (VASP) [13] with the projector augmented wave method [14] to calculate the total energies and the forces. Nonlinear core corrections are applied for all atoms and the Ga-$3d$ electrons are treated as valence states; an energy cutoff of 350 eV and a k-point grid of $4 \times 10 \times 8$ are used in the $3 \times 1 \times 1$ tetragonal cell (24 atoms) with real grid spacings of ≈ 0.08 Å. A modified tetrahedron method [15] was used for the k-point integration in the total energy calculations and the Methfessel-Paxton scheme [16] with a

width of 0.3 eV for the force calculations. This combination of k points and smearing width proved to yield converged values for phonons that are relevant for the free energy. The *ab initio* force constants are calculated using a direct approach with displacements of ≤ 0.1 Å. These were tested to be still within the harmonic regime.

The phonon frequencies and resulting thermodynamics are obtained from the *ab initio* force constants using the **c** + + library S/PHI/NX [17]. The vibrational contributions are determined within the quasiharmonic approximation [18]: the experimental phase transition occurs at constant pressure, i.e., at the equilibrium volume (V_{eq}) for that temperature. This volume is self-consistently determined at each temperature by calculating the phonons at various volumes and minimizing the resulting free energy. Previous studies on a large set of fcc metals showed excellent agreement with experimental data [19].

The magnetic contributions to the free energy can be modeled by constraining the total moment per cell by means of the fixed-spin-moment approach [20]. Although this approach is not expected to reflect all the subtleties related to, e.g., the locality of the moments and the energy spectrum of the spirals at the zone boundaries [21], it captures the essential physics of the current phase transitions. These take place well below the Curie temperature, i.e., at temperatures where fluctuations in the ferromagnetic nature of the phases are less important. Furthermore, the temperature induced changes in the magnetic structure affect mainly the Ni atoms since (i) the Ni-d states dominate the density of states at the Fermi level [4,5] and (ii) the Ni atoms in the $L2_1$ phase do not exhibit stable localized moments on their own, but rather follow the net field of the surrounding Mn moments [21]. The temperature dependence of the magnetization (μ_T) is described using the Kuz'min formula [22] with the experimental Curie temperature $T_C = 376$ K [23] and the parameters $s = 0.1$ and $p = 2.8$. The magnetic contribution to the free energy is then obtained up to first order in μ_T:

$$F(\mu_T, T) = F(\mu_0, T) + (\mu_T - \mu_0) \times \frac{F(\mu_{\mathrm{ref}}, T) - F(\mu_0, T)}{\mu_{\mathrm{ref}} - \mu_0}.$$

Here, $\mu_0 = \mu_{T=0\ \mathrm{K}}$ and μ_{ref} is a reference magnetic moment for which we took $\mu_{\mathrm{ref}} = \mu_{T\approx 270\ \mathrm{K}} = 5\mu_0/6$. The premartensite–austenite energy difference as a function of μ_T confirms that the linear description is well suited. Moreover, the temperature to which the reference magnetic moment corresponds is comparable to the premartensitic transition temperature [2] and so higher order contributions are minimized.

The described approach is carried out for each of the three relevant phases (austenite, premartensite, martensite). This involves full phonon spectra for each phase, multiple volumes and two magnetizations, all requiring a minimum of 9 or 18 supercell calculations (depending on symmetry). The total energies combined with the vibrational and magnetic contributions yield the free energy at each temperature.

In a first step, we determine the equilibrium structures of the austenite and the martensite of Ni_2MnGa by considering all orthorhombic distortions of the cubic $L2_1$ Heusler structure. The cubic phase of the austenite turns out to be a shallow minimum of this energy surface [24] and a tetragonal distortion with $c/a = 1.25$ yields the stable phase at $T = 0$ K in agreement with Ref. [4], which refined the original work on this phase [7,8]. This is the martensite phase as seen by neutron powder diffraction on slightly off-stoichiometric Ni_2MnGa in Ref. [25] and it is the stable phase upon cooling below 128 K in slightly off-stoichiometric Ni_2MnGa according to Ref. [5]. This phase is also used in previous DFT studies [1,10]. The premartensite structure (depicted in Fig. 1) is obtained from a soft phonon analysis [24] of the austenite imaginary frequency at $\mathbf{q} = X_2/3$ (see below). The resulting modulated structure consists of coherent shifts of (110) planes in the $[1\bar{1}0]$ direction with amplitudes of 0.170, 0.150, and 0.153 Å (for the Ni, Mn, and Ga atoms, respectively).

For the phonons, a very good agreement is obtained with the DFT calculations of Bungaro *et al.* [26] and experiment for the austenite [2]. For the TA_2 branch along the [110] direction (see Fig. 2), experiment finds a phonon softening, whereas the DFT calculations consistently yield imaginary phonon frequencies (cf. Ref. [27]). These indicate a lattice instability: the structure can gain energy by moving the atoms along an eigenvector belonging to the imaginary phonons. This lowers the symmetry and results in the modulated structure of the (cubic) premartensite as discussed above. The premartensite phonon spectrum, consequently, shows a sixfold replication relative to the austenite [28] and no imaginary frequencies. No phonons have yet been reported for this structure. The martensite phonon spectrum shows no soft modes either and is in good

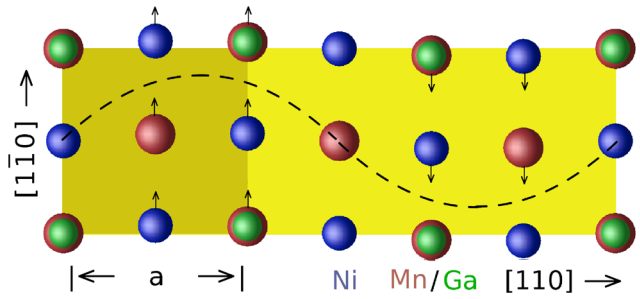

FIG. 1 (color online). Supercell with atomic positions for the 3M premartensite phase as seen from the [001] direction. The cell contains 6 equivalent, but shifted layers along [110]. The corresponding atomic displacements in the $[1\bar{1}0]$ direction (see arrows) follow a sine wave, which is enlarged for better visibility. a is the lattice vector of the austenite tetragonal unit cell (dark area).

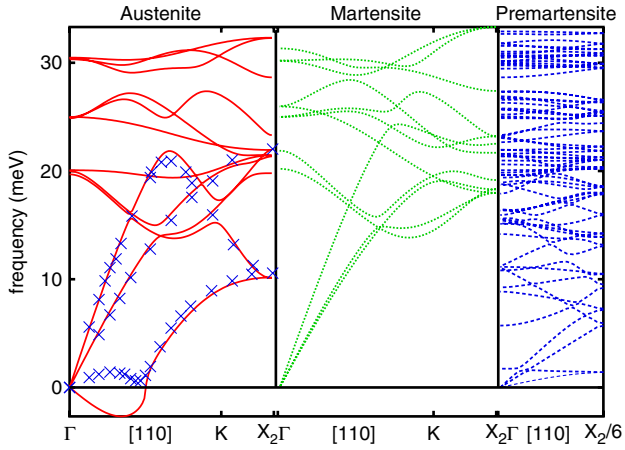

FIG. 2 (color online). Phonon spectrum of the austenite, the unmodulated martensite and the threefold modulated premartensite of Ni_2MnGa in the [110] direction. The lines are *ab initio* data for the $T = 0$ K volumes. Imaginary phonon frequencies of the austenite are plotted negative. The symbols in the austenite spectrum are neutron scattering data [2]. Note that the premartensitic Brillouin zone is sixfold reduced relative to that of the austenite and that its [110] path is enlarged for better visibility.

agreement with previous *ab initio* data [27]. Figure 2 compares the [110] spectra for all three phases.

The free energies are obtained from the full phonon spectra using the partition function [19]. This procedure is straightforward for cases where all phonon frequencies are real, i.e., the martensite and premartensite. An established approach to treat the imaginary frequencies of the austenite [29] is to drop these when integrating over the Brillouin zone, making use of the fact that only a small volume is affected. In fact, manually making all the frequencies real lowers the free energy by only 0.12 meV/atom at 500 K. Figure 3 shows the free energies $F(V_{\mathrm{eq}}, \mu_0, T)$ for all three phases, containing the (quasiharmonic) vibrational, but no magnetic excitations. These free energies yield only one phase transition as a function of temperature: above $T_M \approx 200$ K, the cubic premartensite becomes thermodynamically more stable than the tetragonally deformed martensite, but the transition from the premartensite to the austenite is not yet reproduced. The reason is that entropic contributions from the lattice vibrations (see inset of Fig. 3) are slightly larger for the premartensite than for the austenite, thus making the preference of the premartensite at $T = 0$ K larger with increasing temperature. The premartensite, however, originates from a structural relaxation of the austenite, which should cause the vibrations to become harder rather than softer and so to decrease the entropy. This anomaly was analyzed to be an indirect effect of the larger thermal expansion coefficient of the premartensite. Figure 3 also shows that an estimate of T_M from the austenite-martensite free energy crossing within the quasiharmonic approximation leads to a significant shift to higher temperature ($T_M \approx 270$ K) than the $T_M \approx 175$ K [10] based on the simpler Debye approximation.

In the final step, we include the effect of magnetic excitations as outlined above. The inclusion of these excitations has a striking effect on the free energies and on the resulting phase diagram (see Fig. 4). Most importantly, the magnons make the austenite the stable phase at a temperature of $T_{\mathrm{PM}} \approx 240$ K. Now, imaginary frequencies show up in the premartensite. We estimate the error introduced by dropping these as before; a shift in the transition temperature of maximally +30 K results. The calculated value for the premartensitic transition temperature is, therefore, in very good agreement with those found experimentally [1,2]. The inset of Fig. 4 shows that the entropic

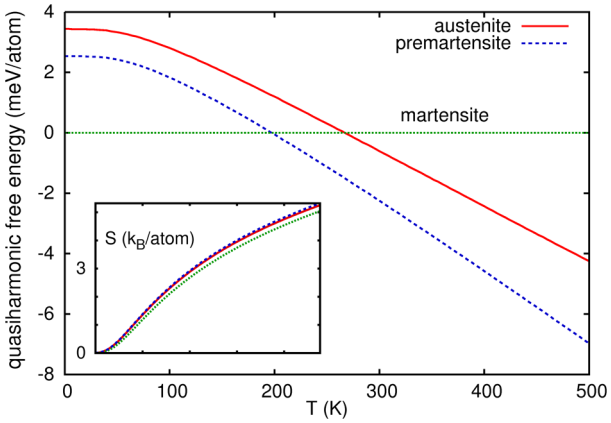

FIG. 3 (color online). Calculated quasiharmonic free energies (F, meV/atom) as a function of temperature (T, K) for the 3 relevant phases of Ni_2MnGa. The respective ground state magnetic moments have been used and data are plotted relative to the martensite. The inset shows the first derivatives $S = -dF/dT$ (k_B/atom) for the same temperature range.

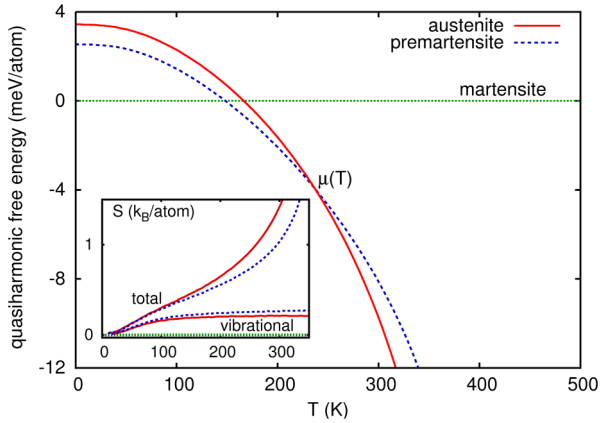

FIG. 4 (color online). Calculated free energies (F, meV/atom) including both vibrational and magnetic excitations as a function of temperature (T, K) for the 3 relevant phases of Ni_2MnGa. The inset shows both the vibrational and the total first derivatives $S = -dF/dT$ (k_B/atom). All data are plotted relative to the martensite.

contributions from both magnons and phonons of the premartensite and austenite only slightly differ. We, therefore, conclude that the existence of the premartensite transition is a delicate interplay of the two excitation mechanisms: the magnetic excitations overcompensate the anomalous vibrational entropies.

The magnetic entropy also stabilizes the premartensite faster relative to the martensite and consequently decreases the martensitic transition temperature by 50 K to $T_M \approx 150$ K. This reflects the experimental situation well, because this study did not consider intermartensitic transitions to the modulated martensite phases [30,31]; these would extend the stability region of the martensite, but the determination of the required phonon spectra at least doubles the supercell sizes and triples the number of atomic displacements.

Similarly to Fig. 3, one can study the stability of the martensite phase due to the magnetic excitations alone. This, again, yields a transition temperature slightly below 200 K, meaning that magnons and phonons are equally important for the martensitic transition.

In conclusion, by combining density functional theory with the quasiharmonic approximation and fixed-spin-moment calculations, we were able to determine the temperature dependence of the free energy including both vibrational as well as magnetic excitations for Ni_2MnGa. Only the combined approach reproduces the rather complex sequence of phase transitions and provides a very good description of the temperature dependent phase diagram of this MSM alloy. Moreover, the mechanisms driving the phase transitions were understood from the subtle differences of vibrational and magnetic effects: they both contribute to the martensitic transition, but the premartensitic transition is driven by the magnetic effects alone, overcompensating those of the vibrations. We believe that this insight will allow for a more systematic search of chemical trends and improvements of the magnetic shape memory properties.

We gratefully acknowledge financial support of the Deutsche Forschungsgemeinschaft within the priority program SPP1239.

*uijttewaal@mpie.de

[1] C. P. Opeil *et al.*, Phys. Rev. Lett. **100**, 165703 (2008).
[2] A. Zheludev, S. M. Shapiro, P. Wochner, and L. E. Tanner, Phys. Rev. B **54**, 15045 (1996).
[3] A. N. Vasil'ev, V. D. Buchel'nikov, T. Takagi, V. V. Khovailo, and E. Estrin, Phys. Usp. **46**, 559 (2003).
[4] A. Ayuela, J. Enkovaara, and R. M. Nieminen, J. Phys. Condens. Matter **14**, 5325 (2002).
[5] P. Entel, V. D. Buchel'nikov, V. V. Khovailo, A. T. Zayak, W. A. Adeagbo, M. E. Gruner, H. C. Herper, and E. Wassermann, J. Phys. D **39**, 865 (2006).
[6] P. J. Brown, A. Y. Bargawi, J. Crangle, K.-U. Neumann, and K. R. A. Ziebeck, J. Phys. Condens. Matter **11**, 4715 (1999).
[7] A. Ayuela, J. Enkovaara, K. Ullakko, and R. M. Nieminen, J. Phys. Condens. Matter **11**, 2017 (1999).
[8] V. V. Godlevsky and K. M. Rabe, Phys. Rev. B **63**, 134407 (2001).
[9] Y. Lee, J. Y. Rhee, and B. N. Harmon, Phys. Rev. B **66**, 054424 (2002).
[10] J. Enkovaara, A. Ayuela, L. Nordström, and R. M. Nieminen, J. Appl. Phys. **91**, 7798 (2002).
[11] M. E. Gruner, W. A. Adeagbo, A. T. Zayak, A. Hucht, S. Buschmann, and P. Entel, Eur. Phys. J. Special Topics **158**, 193 (2008).
[12] J. P. Perdew, K. Burke, and M. Ernzerhof, Phys. Rev. Lett. **77**, 3865 (1996).
[13] G. Kresse and J. Furthmüller, Phys. Rev. B **54**, 11 169 (1996).
[14] P. E. Blöchl, Phys. Rev. B **50**, 17 953 (1994).
[15] P. E. Blöchl, O. Jepsen, and O. K. Andersen, Phys. Rev. B **49**, 16223 (1994).
[16] M. Methfessel and A. T. Paxton, Phys. Rev. B **40**, 3616 (1989).
[17] http://www.sphinxlib.de; S. Boeck and J. Neugebauer, Comput. Phys. Commun. (to be published).
[18] J. Xie, S. de Gironcoli, S. Baroni, and M. Scheffler, Phys. Rev. B **59**, 965 (1999).
[19] B. Grabowski, T. Hickel, and J. Neugebauer, Phys. Rev. B **76**, 024309 (2007).
[20] V. L. Moruzzi, P. M. Marcus, K. Schwarz, and P. Mohn, Phys. Rev. B **34**, 1784 (1986).
[21] J. Enkovaara, A. Ayuela, J. Jalkanen, L. Nordström, and R. M. Nieminen, Phys. Rev. B **67**, 054417 (2003).
[22] M. D. Kuz'min, Phys. Rev. Lett. **94**, 107204 (2005).
[23] P. J. Webster, K. R. A. Ziebeck, S. L. Town, and M. S. Peak, Philos. Mag. B **49**, 295 (1984).
[24] T. Hickel, M. A. Uijttewaal, B. Grabowski, and J. Neugebauer, Mater. Res. Soc. Symp. Proc. E **1050**, BB03-02 (2008).
[25] C. Y. Cong, P. Zetterström, Y. D. Wang, R. Delaplane, R. L. Peng, X. Zhao, and L. Zuo, Appl. Phys. Lett. **87**, 011906 (2005).
[26] C. Bungaro, K. M. Rabe, and A. DalCorso, Phys. Rev. B **68**, 134104 (2003).
[27] A. T. Zayak, P. Entel, J. Enkovaara, A. Ayuela, and R. M. Nieminen, Phys. Rev. B **68**, 132402 (2003).
[28] The Brillouin zone boundary of the $3M$ phase is at $X_2/6$ (as compared to the austenite), because the nonorthogonal fcc lattice vectors make that a [110] lattice modulation of period 3 has 6 equivalent, but shifted atomic planes. The next Γ point is, thus, at $X_2/3$ and equals the soft q point of the austenite as required.
[29] K. Parlinski, Z. Q. Li, and Y. Kawazoe, Phys. Rev. Lett. **78**, 4063 (1997).
[30] P. J. Brown, J. Crangle, T. Kanomata, M. Matsumoto, K.-U. Neumann, B. Ouladdiaf, and K. R. A. Ziebeck, J. Phys. Condens. Matter **14**, 10 159 (2002).
[31] V. A. Chernenko, C. Seguí, E. Cesari, J. Pons, and V. V. Kokorin, Phys. Rev. B **57**, 2659 (1998).